Chemical Papers (2020) 74:2389–2401
https://doi.org/10.1007/s11696-020-01087-4

ORIGINAL PAPER

DFT analysis and electronic properties, and synthesis of tetra (9-phenyl-9H-xanthen-9-yl) oxy peripheral-substituted zinc phthalocyanine

Derya Güngördü Solğun[1] · Mehmet Salih Keskin[2] · Ümit yıldıko[3] · Mehmet Salih Ağırtaş[1]

Received: 1 August 2019 / Accepted: 30 January 2020 / Published online: 7 February 2020
© Institute of Chemistry, Slovak Academy of Sciences 2020

Abstract

The 4-((9-phenyl-9H-xanthene-9-yl) oxy) phthalonitrile compound was synthesized and characterized as starting material. Zinc phthalocyanine was obtained by reaction of 4-((9-phenyl-9H-xanthen-9-yl) oxy) phthalonitrile with $Zn(CH_3COO)_2$. Novel compounds were characterized using mass spectra, UV–Vis spectroscopy, ^{1}H-NMR, ^{13}C NMR, and infrared spectroscopy. The fluorescence, emission, excitation, and absorption spectra of the zinc phthalocyanine compound were studied in tetrahydrofuran (THF). The determination of these properties is very useful for photodynamic therapy applications. Also, zinc phthalocyanine (Zn-Pc) was optimized with the basic set of 6-311G and LanL2DZ of the Density functional theory (DFT). The energy band-gap HOMO–LUMO of the molecule was determined. Chemical indices were calculated using HOMO–LUMO energies. The electrophilic region and the nucleophilic region were defined from the molecular electrostatic potential (MESP) maps. Dipole moment components have been calculated and can be considered as potential candidates for the design of non-linear optical materials.

Keywords Phthalocyanine · Fluorescence · Synthesis · Solubility · Computation · Non-linear

Introduction

Phthalocyanines are a class of compounds that are not naturally found in nature, but are widely synthesized and investigated. Perhaps, the most important feature of them is their electronic structure. This interesting structure of phthalocyanines finds application in areas such as sensor (Diab et al. 2019), catalyst (Farahmand et al.2019; Nesterov et al.2018), dye (Agirtas and Yildiko 2008), non-linear optic (Savelyev et al. 2019), electrochromic (Wong et al. 2019), solar cell (Güngördü Solğun et al. 2019), conductivity (Agırtas 2007), liquid crystals (Makhseed et al. 2004), photodynamic therapy of cancer (Hodgkinson et al. 2017), anti-microbial (Lin et al. 2018), antioxidant(Ağırtas et al. 2013), and DNA binding (Gerasymchuk et al.2018; Arslantas and Agirtas 2018). Different phthalocyanine derivatives are tested for these applications and are the basis for determining new properties. Zinc phthalocyanine compounds have been applied in a wide range of scientific research fields, including materials such as photochemical, photodynamic therapy, and biomedical purposes, including near IR absorption and fluorescent agent properties (Lv et al. 2013; Li et al. 2019). Although phthalocyanines have been widely accepted as technological products, their properties are not adequately explored. In this sense, the need to investigate new features continues. The synthesis of novel-substituted phthalocyanines provides important contributions to the above-mentioned purposes. In particular, Zn (II) phthalocyanine compounds are preferred, because they are diamagnetic for light-sensitive sensors (Kluson et al. 2008; Weijer et al. 2015). Here, the synthesis and optimization of this zinc phthalocyanine complex provides preliminary information as to whether it is suitable as a sensor. In addition to the spectral properties of this zinc phthalocyanine compound, the support of the boundary orbitals with theoretical research on HOMO–LUMO energies makes certain objectives (such

✉ Mehmet Salih Ağırtaş
salihagirtas@hotmail.com

[1] Department of Chemistry, Faculty of Science, Van Yuzuncu Yıl University, 65080 Van, Turkey

[2] Department of Basic Education, Faculty of Education, Siirt University, Siirt, Turkey

[3] Architecture and Engineering Faculty, Department of Bioengineering, Kafkas University, Kars, Turkey

as semiconductor, non-linear) (Basiuk et al. 2019; Krishnan et al. 2017; Nečedová et al. 2017; Thimiopoulos et al. 2019). However, the examination of the structure interactions that are bound to the ligands is useful in that they are the basis of the molecule's usage areas. Therefore, the DFT study of the newly synthesized phthalocyanine compound is useful.

This present study reports the characterization and synthesis of phthalonitrile and zinc phthalocyanine compounds containing (9-phenyl-9H-xanthene-9-yl) oxy substituents. The fluorescence emission and extinction measurements of this phthalocyanine compound in THF were made. Also, absorption measurements of the compound at different concentrations indicate that the compound acts as a monomer in THF. This feature indicates that the compound may be a sensor agent for photodynamic applications. Analysis of the highest occupied molecular orbital (HOMO) and lowest free molecular orbital (LUMO) energies, MEP distribution of the molecule, and the Mulliken population analysis of the atomic loads in various molecular atoms are given.

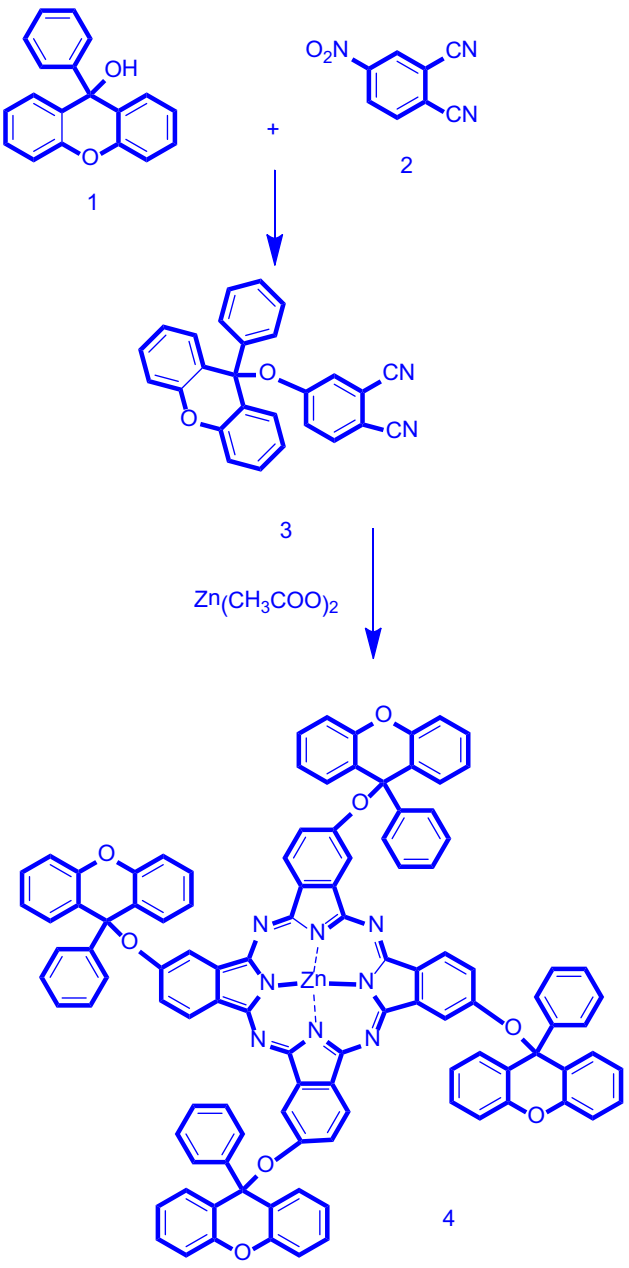
Experimental

Materials

The chemicals required in the experimental procedures were used as received without purification. High-resolution mass spectra were recorded by LC–MS TOF electrospray ionization technique (LC/MS (Thermo Scientific, TSQ-Quantum Access). ^{1}H and ^{13}C NMR spectra were recorded on an Agilent 400 MHz spectrometer. Electronic absorption measurements were performed with a Hitachi U-2900 Spectrophotometer. Fluorescence excitation and emission spectra were recorded on a shımadzu RF-6000 spectrofluorophotometer using 1 cm pathlength cuvettes at room temperature. Infrared measurements were performed with a Thermo Scientific FT-IR spectrophotometer.

4-((9-Phenyl-9H-xanthen-9-yl) oxy) phthalonitrile (3)

A mixture of 9-phenyl-9-xanthenol **1** (0.500 g, 1.823 mmol) and 4-nitrophthalonitrile **2** (0.575 g, 1.823 mmol) in 20 mL dimethylformamide (DMF) was continued for 15 min at room temperature under nitrogen atmosphere. Subsequently, K_2CO_3 (0.795 g, 5.76 mmol) was added to the reaction medium over a 2 h period. The reaction was continued for 7 days at room temperature. To precipitate the product, this mixture was poured into approximately water (200 mL) and stirred for some time. The precipitate formed was filtered off, and then washed with purified water to neutralize. Product was washed by diethyl ether. The resulting product was dried in a vacuum oven. Product is soluble in acetonitrile (hot), acetone, and dimethyl sulfoxide (DMSO). Yield: 0.156 g, Mp: 220 °C. $C_{27}H_{16}O_2N_2$:400.43 g/mol. HRMS (ESI); (M + H) calc. for $C_{27}H_{16}O_2N_2$: 400.43; found: 423.11 $[M+Na]^+$. IR: spectrum (cm^{-1}):3074, 2233, 1598, 1477, 1442, 1311, 1290, 1242, 1155, 1097, 1026, 902, 869, 808. ^{1}H NMR (400 MHz, DMSO-d_6): (δ: ppm) 9.03, 8.68, 8.66, 8.43, 8.42, 8.23, 8.21, 8.04, 7.70, 7.68, 7.34, 7.32, 7.31, 7.29, 7.27, 7.23, 7.22, 7.20, 7.18, 7.12, 7.11, 7.09, 7.07, 7.05, 6.74, 3.37, 3.32, 2.48. ^{13}C NMR (400 MHz, DMSO-d6): (δ: ppm) 150.15, 149.52, 137.03, 136.11, 129.23,



Scheme 1 Schematic representation of the synthesis of compounds (**3–4**)

128.32, 125.97, 123.77, 116.26, 69.09, 40.58, 40.37, 40.16, 39.95, 39.74, 39.53, 39.33.

[Tetrakis-(9-phenyl-9H-xanthen-9-yl)oxy phthalocyaninato] zinc (II) (4)

To synthesize the phthalocyanine complex, compound **3** (0.040 g, 0.100 mmol) and Zn $(CH_3\ COO)_2$ (0.015 g, 0.082 mmol) were added to the reaction vessel. The mixture was heated at 250°°C for 6 min. The temperature of the mixture was allowed to warm to room temperature. For purification, it was washed with different solvents such as hot acetonitrile. TLC follow-up was performed for the purification process. This zinc phthalocyanine complex is well soluble in polar organic solvents such as THF, DMF, and DMSO. Yield: 0.016 g (38.09%). HRMS (ESI); (M + H) calc. for $C_{108}H_{64}N_8O_8Zn$: 1664.41; found: 1687.39 $[M + Na]^+$. UV–Vis) (THF) λ_{max}, nm (log ε): 676 (5.23), 640 (5.04), 344 (5.12). ^{1}H NMR (400 MHz, DMSO-d_6): (δ: ppm) 8.65, 8.42, 8.01, 7.78, 7.73, 7.51, 6.85, 6.63, 3.33, 2.48. IR spectrum (cm^{-1}): 1587(C=C), 1483, 1398, 1276, 1247 (Ar–O–Ar), 1083, 1047, 958, 850, 746.

Results and discussion

The synthesis reaction diagram of the 4-((9-phenyl-9H-xanthen-9-yl) oxy) phthalonitrile (**3**) and zinc (II) phthalocyanine (**4**) is shown in Scheme 1. The 4-((9-phenyl-9H-xanthen-9-yl)oxy)phthalonitrile (**3**) was accomplished by a base-catalyzed nucleophilic aromatic nitro displacement reaction between 9-phenyl-9-xanthenol **1** and 4-nitrophthalonitrile **2** in the presence of dry K_2CO_3 in dry DMF under a N_2 atmosphere for 7 day at rt. The phthalocyanine (**4**) was obtained by the reaction of 4-((9-phenyl-9H-xanthen-9-yl) oxy) phthalonitrile (**3**) with $Zn(CH_3COO)_2$. Purification of the phthalocyanine complex was followed by washing with some solvents and followed up with TLC. The characterization of these compounds was achieved by mass, FT-IR, ^{1}H NMR, and UV–Vis spectroscopic methods.

The IR spectrum in the vibrations of the functional groups gives important information. One of the most characteristic groups for the newly synthesized phthalonitrile derivative is nitrile peak. This peak was observed at 2233 cm^{-1} as expected. Another characteristic vibration peak is aromatic in 3074 cm^{-1}, C=C vibrations in 1598 cm^{-1}

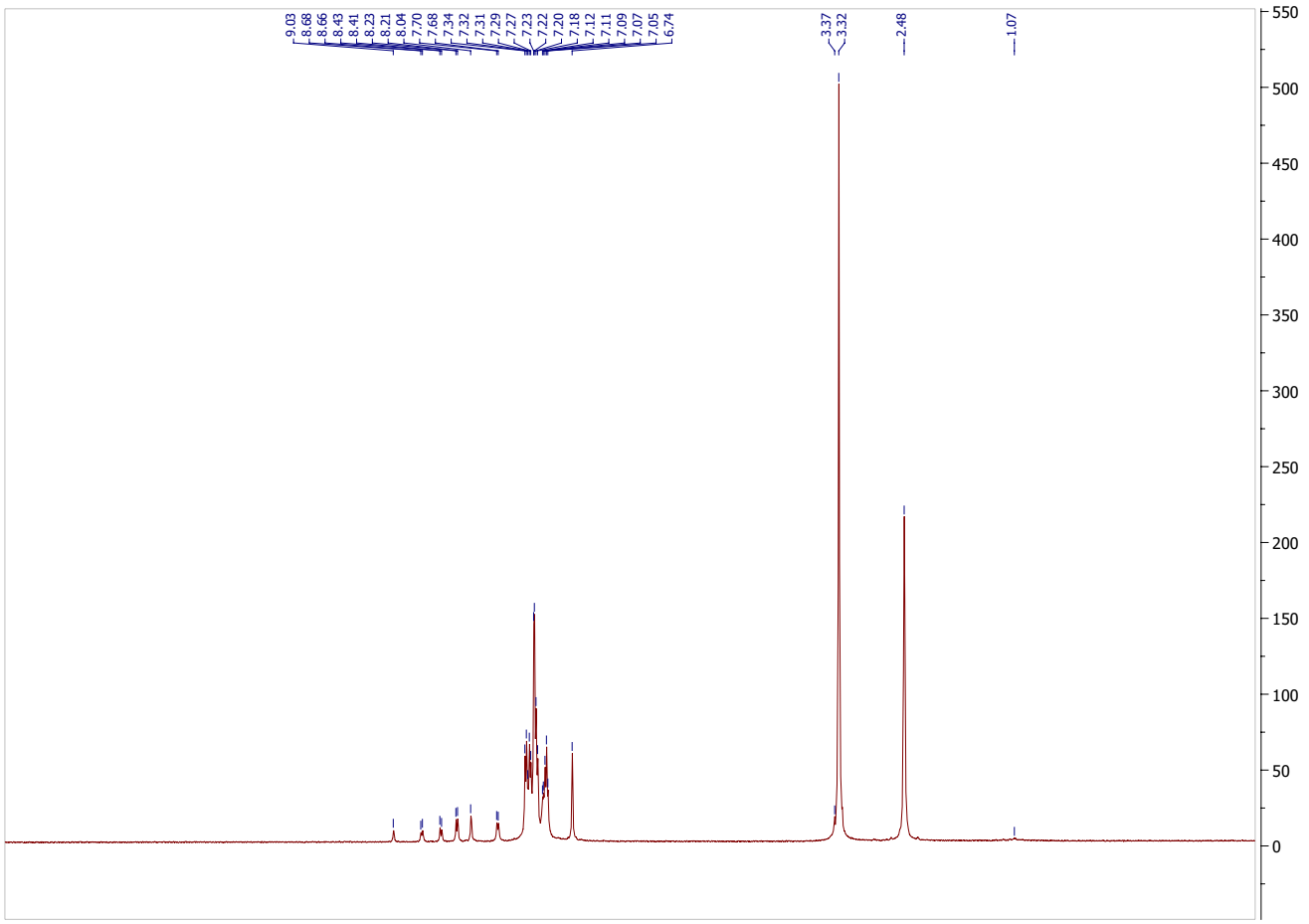


Fig. 1 ^{1}H-NMR spectra of compound **3**

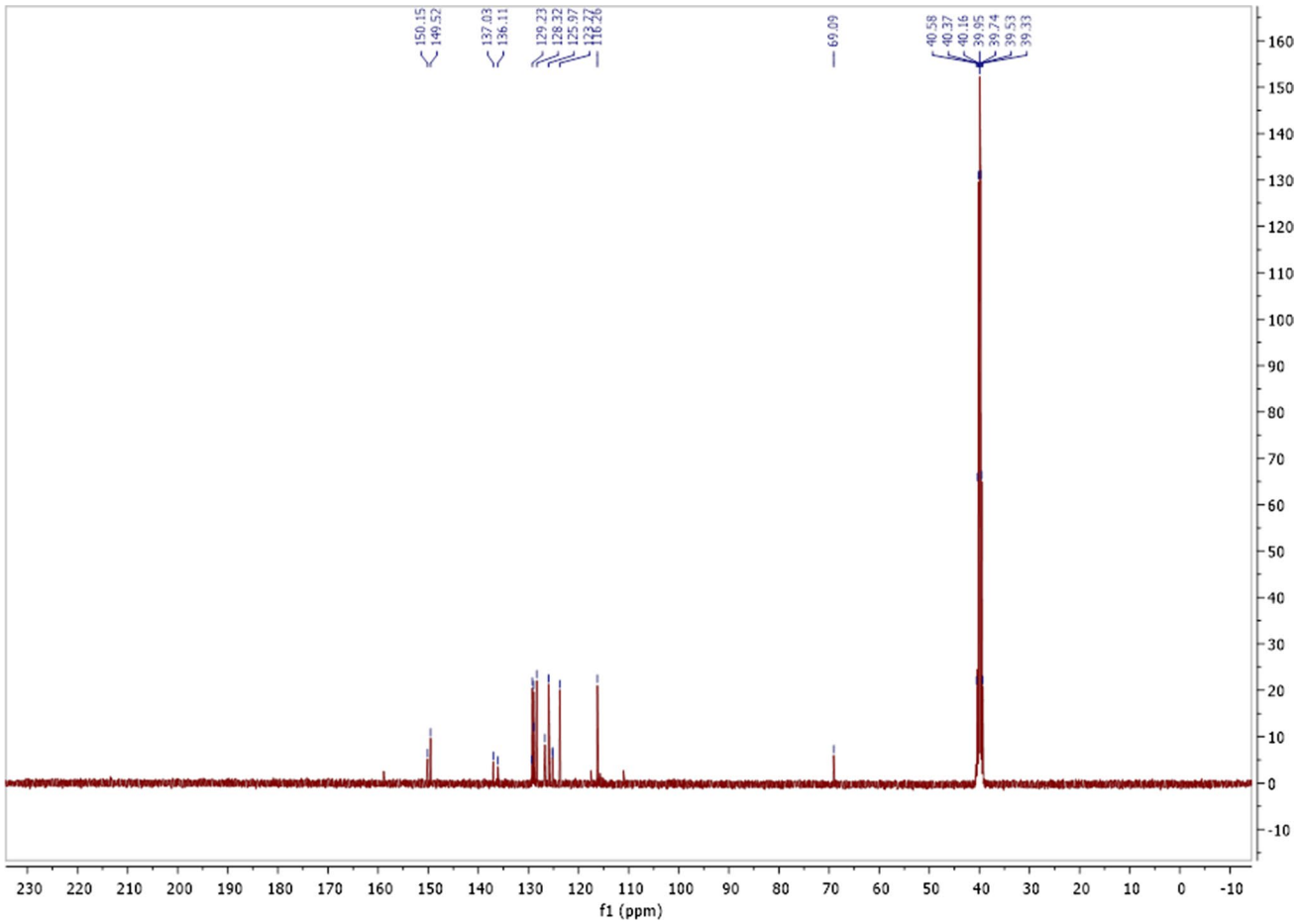


Fig. 2 ^{13}C-NMR spectra of compound **3**

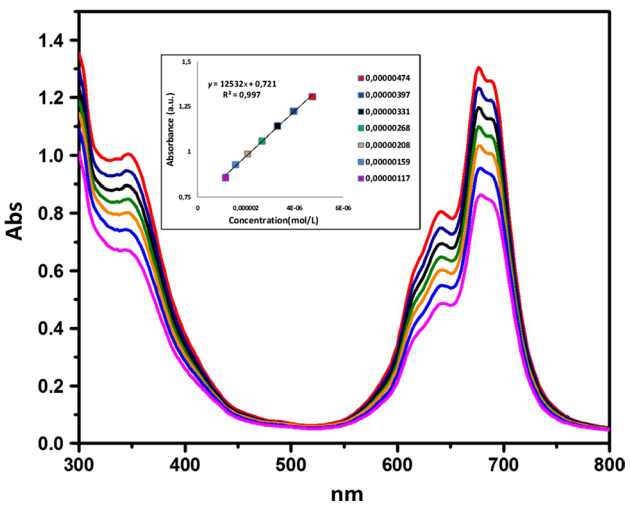


Fig. 3 Aggregation properties of zinc phthalocyanine at different concentrations

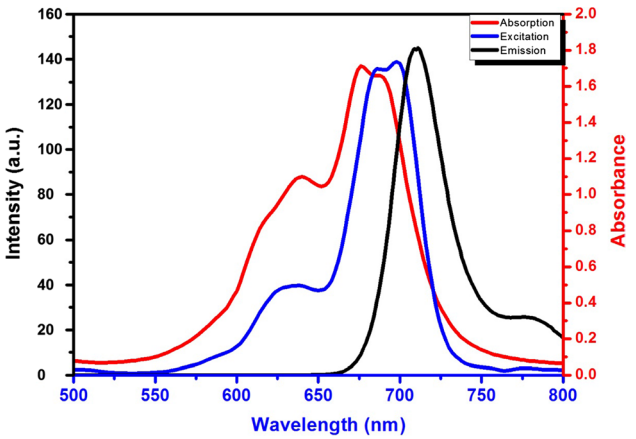


Fig. 4 Emission, excitation, and absorption spectra of zinc phthalocyanine

and Ar–O–Ar vibration in 1242 cm^{-1}. These values correspond to the vibration frequencies in the structure. After the formation of zinc (II) phthalocyanine, the IR spectra are

Table 1 Theoretically obtained bond lengths (Å,°) of the molecule (DFT)

Atom groups		Bond lengths	
		6-311G	LanL2DZ
1	C4–N7	1.33575	1.34349
2	Zn41–N5	2.00400	2.02285
3	C15–C32	1.39219	1.40081
4	Zn41–N12	2.00402	2.02297
5	Zn41–N18	2.00609	2.02501
6	Zn41–N24	2.00389	2.02271
7	O109–C27	1.40004	1.40187
8	C56–O74	1.40831	1.41046
9	C90–O108	1.40584	1.40831
10	C38–H51	1.08138	1.08593
11	C30–O144	1.39972	1.40077
12	C159–O177	1.40210	1.40469
13	O75–C34	1.40015	1.40164
14	N7–C8	1.33614	1.34374
15	C10–C11	1.46166	1.47028
16	C23–N24	1.38553	1.39266
17	N5–Zn41	2.00400	2.02285
18	N19–C20	1.33787	1.34555
19	C11–N13	1.33203	1.34350
20	C117–H120	1.08166	1.08729

Table 2 Theoretically obtained bond dihedral (Å,°) of the molecule (DFT)

Atom groups		Bond lengths	
		6-311G	LanL2DZ
1	C20–N19–C17–C16	179.46	179.87
2	Zn41–N18–C14–C15	179.48	179.96
3	C15–C16–C32–H45	179.82	179.88
4	Zn41–N12–N5–C11	179.91	179.92
5	C30–C31–O144–O128	-170.27	− 173.83
6	C20–N24–N19–C17	− 0.089	0.14799
7	C8–C9–C10–C28	− 179.99	− 179.98
8	C16–C17–C31–H44	0.22901	− 0.02853
9	C38–C39–H51–O178	− 0.04219	0.16325
10	C4–N7–C8–C9	179.97	179.84

Table 3 Theoretically obtained bond angles of the molecule (Å,°) (DFT)

Atom groups		Bond angles	
		6-311G	LanL2DZ
1	C1–N5–C4	109.12041	109.40114
2	N18–Zn41–N12	89.98389	89.97140
3	C11–Zn41–N12	125.41597	125.27074
4	C39–O178–C162	124.29973	124.28883
5	C125–O143–C129	119.32546	119.23657
6	N7–C8–N12	126.03788	126.82842
7	C21–C22–C23	106.73210	106.76152
8	C27–H43–C28	122.75649	123.05841
9	C21–C36–H47	120.68092	120.67177
10	C34–O75–C59	126.87853	127.02901
11	N19–C20–N24	126.86688	126.85115
12	N13–C11–C14	125.21805	125.57494
13	C1–N5–Zn41	125.59297	125.45243
14	C128–C145–C146	122.43573	122.42659
15	C30–O144–C31	113.66279	113.46719
16	N5–N24–Zn41	89.96360	89.95491
17	O109–C27–C93	127.35722	127.05985
18	C10–N13–C11	124.33980	124.57447
19	N5–C1–N6	126.74031	126.70981
20	C8–C9–C10	35.87603	107.07837

specifically related to the loss of specific CN peak and some shifts in other vibrations. Zinc (II) phthalocyanine **4** for C=C 1587 cm^{-1} and Ar–O–Ar vibration is seen to have shifted to 1247 cm^{-1}.

When the ^{1}H NMR spectrum of Compound **3** is examined, the protons belonging to the aromatic ring according to the structure of the molecule are observed in the range of 9.03–7.22. There are no aliphatic protons in the structure of the molecule. Only the peaks of the DMSO-d_6 solvent are seen as 3.32 and 2.48 ppm. In the ^{13}C NMR spectrum of the same compound in DMSO-d_6, the aromatic protons 150.15, − 116.26, and 69.09 ppm are observed, while the peak of the solvent is seen as a peak in the peak of 39.95 ppm. Figures 1, 2 show the proton and carbon NMR spectra of 4-((9-phenyl-9H-xanthen-9-yl) oxy) phthalonitrile **3**. In the ^{1}H NMR spectrum of zinc phthalocyanine compound **4**, some peaks are shifted, and intermediate protons are observed to be in the range of 8.65–6.63. Furthermore, peaks of the DMSO-d_6 solvent are observed in 3.33–2.48.

The electron density of the phthalocyanine compounds 18 π gave distinctive properties to the phthalocyanines. One of the most commonly used devices in determining these discriminative behaviors is UV–visible spectroscopy. Q and B absorption bands, which are frequently mentioned in electronic literature and which come from electronic transition, give information about whether phthalocyanines bind metal about ring structure. The Q and B absorption bands for this phthalocyanine are 676 and 344 nm, respectively. The absence of cleavage in the Q band indicates that phthalocyanine binds metal (Laajimi et al. 2019). Electronic absorption spectroscopy has been widely used to determine whether the structure contains metal. In this study, electronic absorption measurements of zinc phthalocyanine compound were

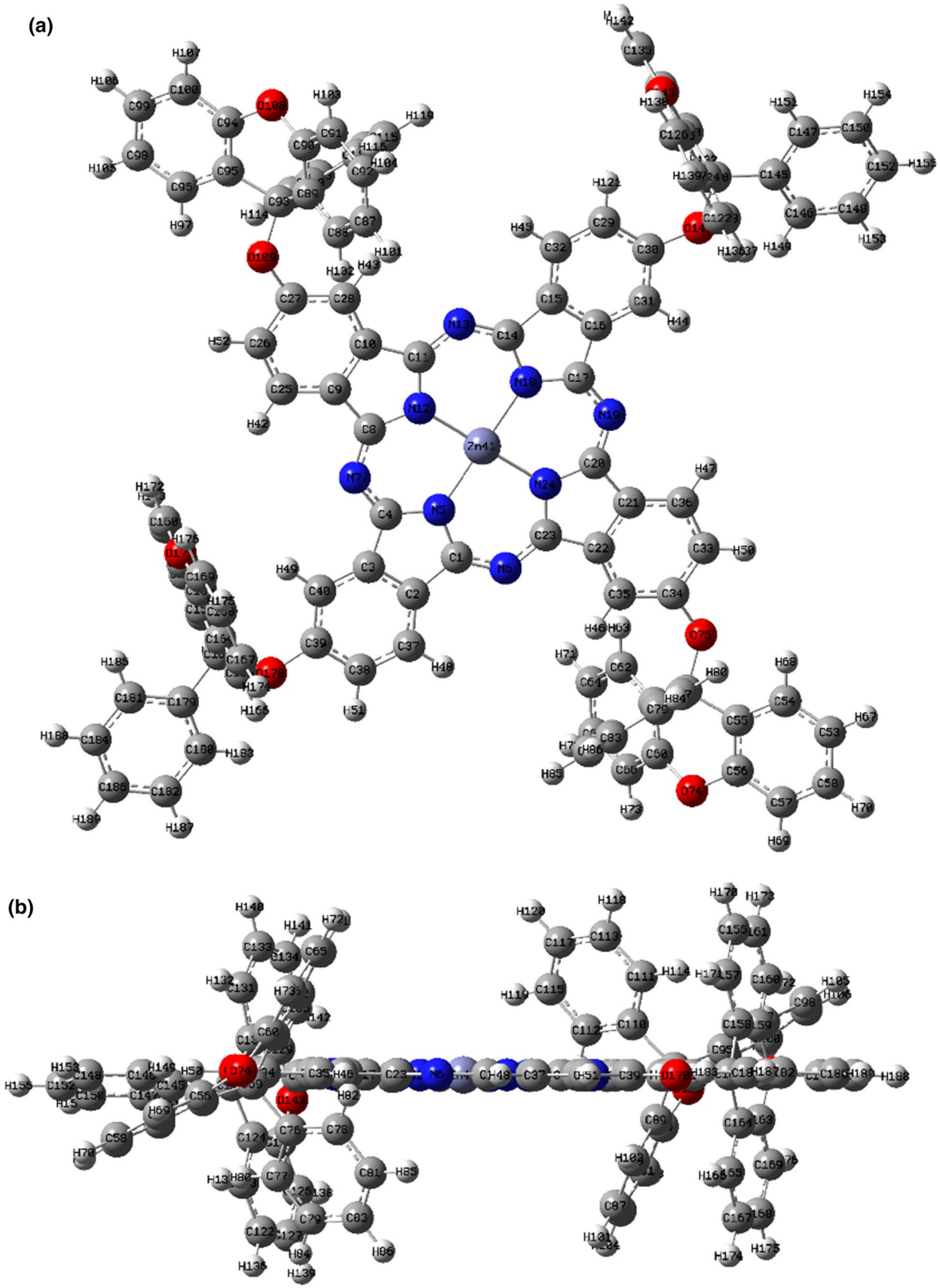


Fig. 5 The optimized structure of the compound using LanL2DZ base clusters

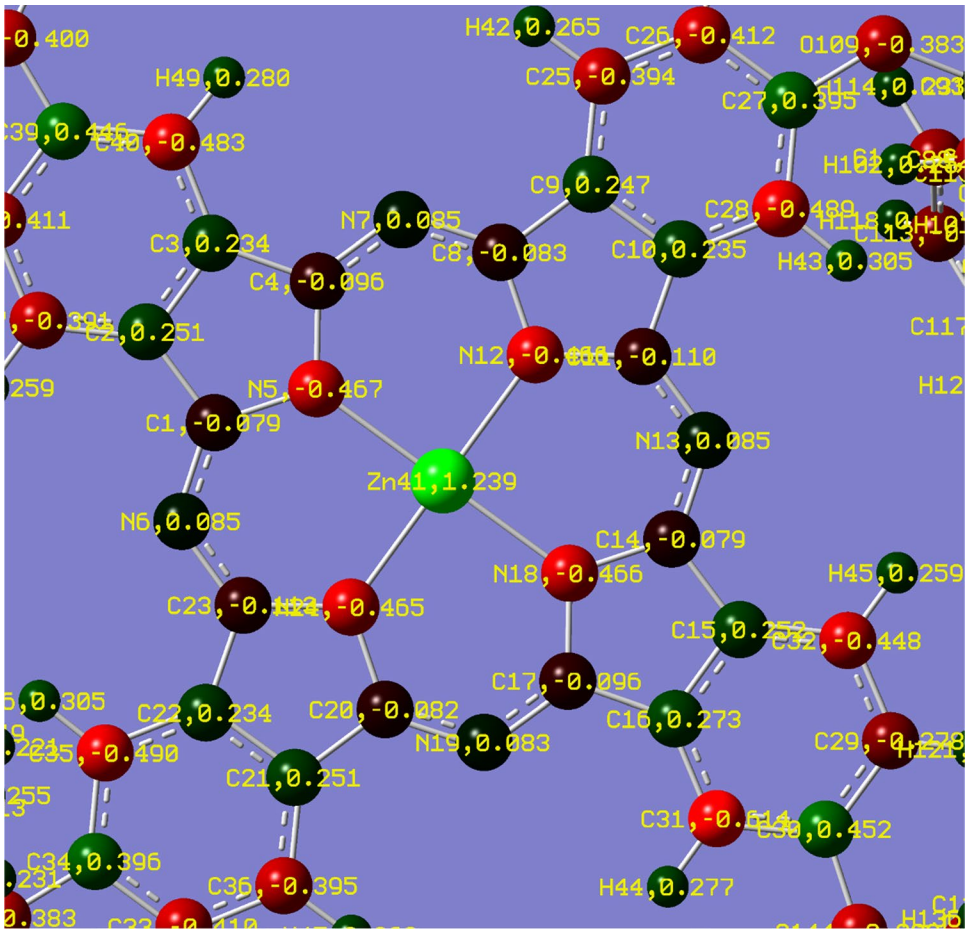


Fig. 6 Mulliken atom charges of compound 4 calculated at DFT/B3LYP/3-21G (+) level

measured for different concentrations in THF. It was found that the compound was not aggregated (Fig. 3).

Fluorescence molecules in general; bio-labeling, enzyme–substrate, environmental indicator, cell organelle labeling, disease diagnostics, organic radiation-emitting diodes, sensor agents, such as finding a wide range of common uses in chemistry, biology, and physics, and has become an integral part of the science. Tetrahydrofuran was used for the fluorescence absorption, excitation, and emission spectra of the zinc phthalocyanine compound **4**. The spectra observed are shown in Fig. 4. Stokes shifts are located within the observed interval for phthalocyanines. The excitation spectra show some similarities with the absorption spectra (Fig. 4). Fluorescence Stokes shift value of zinc phthalocyanine is found as 8 nm. Excitation gives λ_{ex} (nm) 698, while emission gives 706 nm fluorescence. The observed Stokes shift of zinc phthalocyanine compound **4** is near to standard zinc phthalocyanine (StdZnPc) (Saka et al. 2011).

The form of this compound is more economical than the conventional methods. It provides advantages such as short-term synthesis and no need for solvent. The absence of the solvent in the environment also facilitates purification. The fact that this phthalocyanine compound exhibits non-aggregate and fluorescence properties is advantageous for applications such as photodynamic therapy.

Theoretical results

Theoretical calculations were performed using the Density Functional Theory (DFT) method applied in the Gaussian 09 calculation package (Frisch et al. 2009).

Molecular geometry and Mulliken charge distribution analysis

B3LYP is known to work well and consistently in quantum chemical calculations (Abkari et al. 2016; Zhao et al. 2018). This method has been used in many studies on metallo-organic compounds. Verifies the linearity of the core and the planarity of the environment with optimized structures; it is also important to understand the behavior of the more dense phases of complexes.

For some selected atomic groups, the optimized Zn-Pc parameters calculated using the 6-311G (+) and the LANL2DZ base set by the B3LYP method are listed in Tables 1, 2 and 3. The structure of the molecule consists of planar

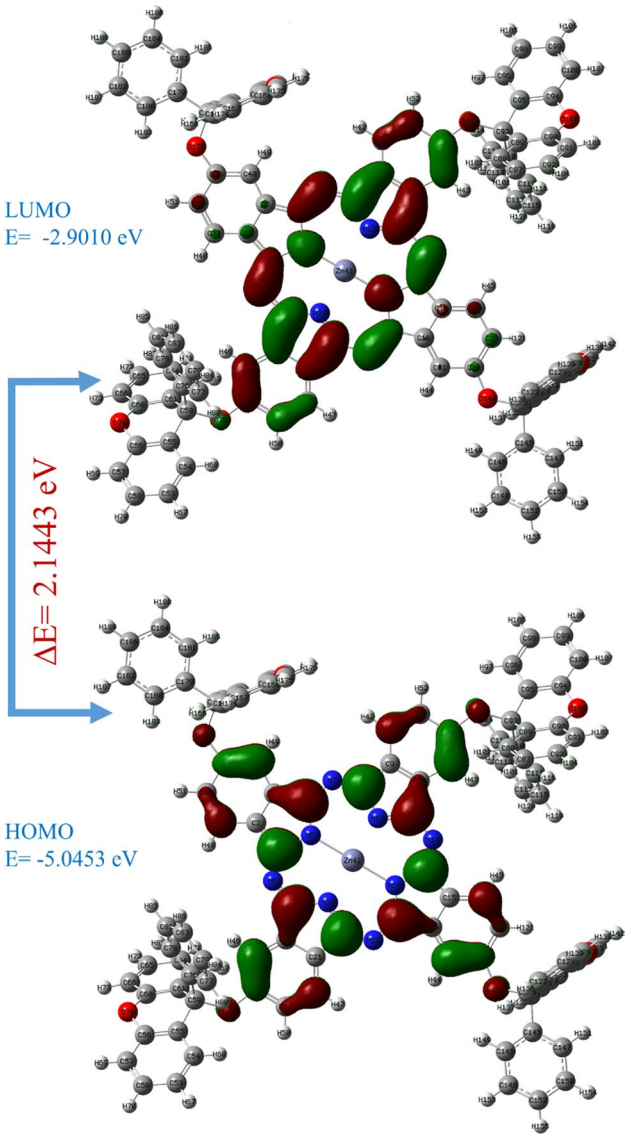


Fig. 7 Compound 4 HOMO–LUMO energy maps and band gap

Table 4 Comparison of HOMO, LUMO, energy gaps (Δ), and related DATPA (au) molecular properties

Molecules energy	6-311G	LanL2DZ
E_{LUMO}	−2.9035	−2.9010
E_{HOMO}	−5.0720	−5.0453
Energy gap (Δ) E_{HOMO}–E_{LUMO}	2.1685	2.1443
Ionization potential (I = −E_{HOMO})	5.0720	5.0453
Electron affinity ($A = -E_{LUMO}$)	2.9035	2.9010
Chemical hardness ($\eta = (I - A)/2$)	1.0842	1.0721
Chemical softness ($s = 1/2\ \eta$)	0.5421	0.5360
Chemical potential ($\mu = (I + A)/2$)	3.9877	3.9776
Electronegativity ($\chi = (1 + A)/2$)	1.9517	1.9505
Electrophilicity index ($\omega = \mu^2/2\ \eta$)	14.6668	14.7586

Table 5 DFT belong to the basic set B3LYP/6-311G (d, s) and LanL2DZ, electricity calculated dipole moments (Debye), (au) polarizability, β components, and β tot DATPA value

Parameters	6-311G	LanL2DZ
μ_x	0.8532	0.8669
μ_y	0.3560	0.3629
μ_z	0.2628	0.1622
$\mu_{(D)}$	0.9611	0.9537
α_{xx}	−675.4576	−658.2325
α_{yy}	−686.4507	−672.9340
α_{zz}	−683.6208	−670.1446
α_{XY}	−19.9769	−23.8451
α_{XZ}	2.8478	1.9240
α_{YZ}	−15.5961	−17.8228
α (au)	−681,8430	−667,1037
β_{XXX}	−23.1564	−38.7877
β_{XXY}	39.6376	41.8981
β_{XYY}	−4.3915	−5.2537
β_{YYY}	−83.5606	−84.1007
β_{XXZ}	−20.2764	9.4686
β_{XYZ}	5.4769	0.6493
β_{YYZ}	3.4680	−9.4349
β_{XZZ}	64.0810	61.8927
β_{YZZ}	41.7291	32.7330
β_{ZZZ}	19.6878	12.6149
β (esu)	3.6×10^{-21}	3.2×10^{-21}

phthalocyanine core and bent side groups (Fig. 5). For Zn-Pc, the binding distance of the central atom to the nitrogen atoms is between 2.004 and 2.022 Å in the base sets 6-311G and LanL2DZ for Zn41–N12, respectively. In the study with the LanL2DZ basic set, the phthalocyanine nucleus was found to be slightly larger. Other bond lengths are listed in the comparative and normal range. The Zn-Pc constructs optimized with atomic loads of B3LYP/LanL2DZ and Muliken are shown in Fig. 6.

The selected atomic groups Zn41–N18–C14–C15 and C20–N19–C17–C16 dihedral angles were calculated to be close to 180°. The angles indicated in Table 2 indicate that the phthalocyanine nucleus is planar. The two basic sets gave a concordant result.

Mulliken load distribution for zinc atom, Zn41 (1.239), and the nitrogen attached to the central atom were calculated as N12 (−0.466), N24 (−0.465), respectively. Some of the C atoms in the phthalocyanine nucleus were positive and some were negative.

This phthalocyanine molecule, which is theoretically studied, has 189 atoms. Mulliken load distribution calculations, bond angles and lengths for this phthalocyanine molecule are the parameters that confirm and optimize the

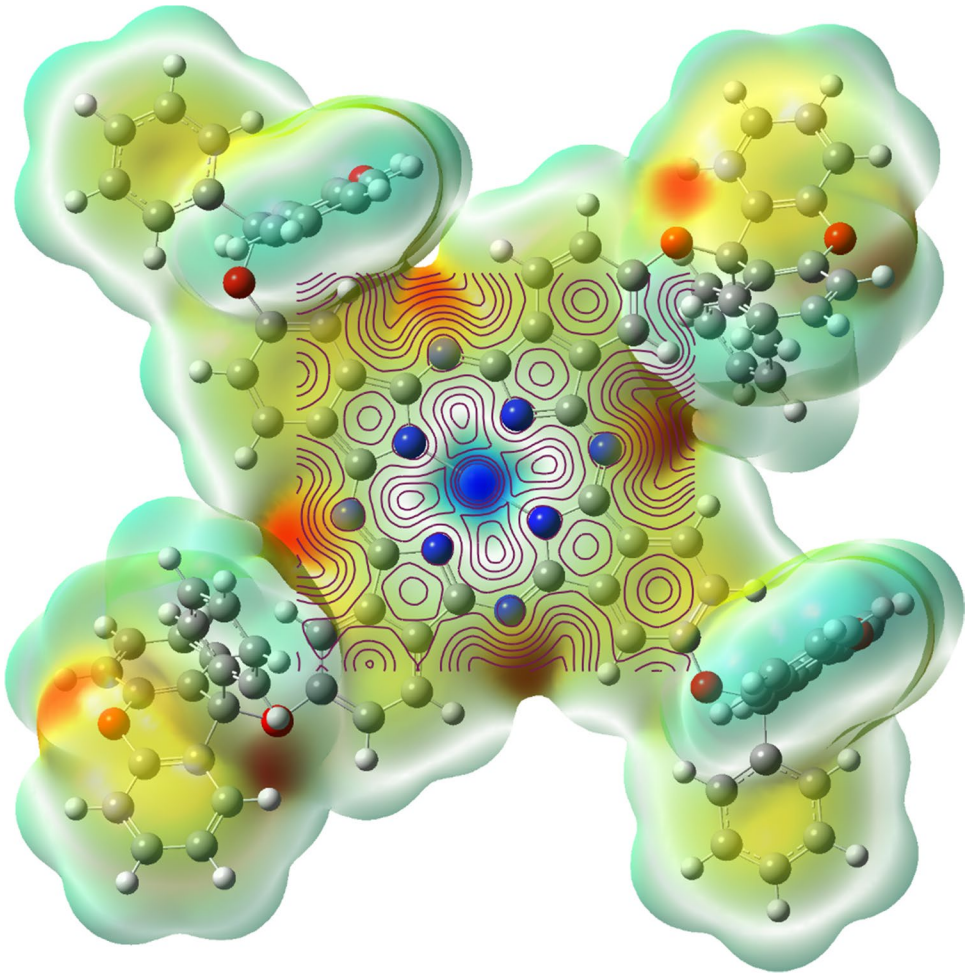


Fig. 8 Molecular electrostatic potential mapped of compound **4**

structure. Modeled data support experimental data for synthesized zinc phthalocyanine compound.

Frontier molecular orbitals [HOMO–LUMO]

Some electronic features for the optimized compound **4** have also been reported herein, and HOMO and LUMO density trajectory maps are given in Fig. 7. In addition, ELUMO + 1 and EHOMO − 1 energy values of the compounds were also calculated. In the phthalocyanine molecule; EHOMO = − 5.0720 eV—ELUMO = − 2.9035 eV, calculated. For other orbits: for Zn-Pc, the value of EHOMO − 1 = − 6.1336 eV ELUMO + 1 = − 2.9007 eV was calculated. HOMO and LUMO orbitals determine the way the molecule interacts with other species. The determination of HOMO–LUMO energies also helps to understand the chemical stability of a molecule for a parameter known as chemical hardness (η) (Chen and Wang 2019; Prabhaharan et al.2015). The molecules with large HOMO–LUMO energy gaps are considered to be soft molecules with molecules of hard molecules, small HOMO–LUMO energy cavities (Table 4.). Table 3 shows the chemical reactivity indices.

Quantum chemical calculations are for a single molecule in gaseous state. However, there may be deviation from the experimental values recorded in the presence of intermolecular interactions (Table 5).

Molecular electrostatic potential (MEP)

In this study, molecular electrostatic potential (MEP) maps were extracted with both basic sets. As shown in Fig. 8, the MEP maps of LanL2DZ and 6-311G were mapped. The MEP map shows that the central atom has positive region fields characterized by blue color around it (Sayin and Karakaş 2015; Yankova et al. 2017). Also, the hydrogen atom in the ligands carries the maximum strength of the positive charge (dark blue). The aromatic ring region shows an almost neutral potential, most of which is represented by green color.

Table 6 Selected NBO results show the formation of Lewis and non-Lewis orbitals for compound 4 (Zn-Pc) using the B3LYP/6-311 G ++ (d, p) theory level

NBO(i)	Type	ED/e	NBO(j)	Type	ED//e	$E(2)^a$(Kcal/mol)	$E(j)$–$E(i)^b$(a.u.)	$F(i,j)^c$(a.u)
C1–N6	σ	1.98029	C1–C2	σ*	0.04118	1.32	0.042	1.65
			C4–N5	σ*	0.04857	2.54	1.26	0.051
			N6–C23	σ*	0.02502	1.07	1.34	0.034
			C22–C23	σ*	0.04202	3.37	1.31	0.060
N6–C23	σ	1.98030	C1	π*	0.00633	2.36	1.47	0.053
			C22	σ*	0.01126	1.82	1.56	0.048
			C1–C2	σ*	0.04118	3.33	1.32	0.060
			C20–N24	σ*	0.04881	2.53	1.26	0.051
			C22–C23	σ*	0.04202	1.62	1.31	0.041
N6–C23	π	1.70249	C1		0.00535	2.01	0.71	0.037
			C1–N5	π*	0.59327	36.85	0.27	0.097
			C21–C22	π*	0.46013	10.12	0.35	0.055
C8–N12	σ		C9–C25	σ*	0.02257	4.18	1.34	0.067
			C11–N13	σ*	0.02515	5.43	1.29	0.075
C8–N12	π	1.77064	C4–N7	π*	0.44913	7.24	0.31	0.045
			C11–N13	π*	0.44958	32.12	0.31	0.094
			C4–N7	π*	0.44913	170.96	0.03	0.088
			C9–C10	π*	0.45947	52.99	0.07	0.076
C11–N12	σ	1.98016	N7–C8	σ*	0.02520	5.30	1.30	0.074
			C10–C28	σ*	0.02162	4.11	1.37	0.067
C15–C16	π	1.58683	C14–N18	π*	0.58850	33.72	0.21	0.078
			C17–N19	π*	0.44558	26.71	0.24	0.071
			C29–C32	π*	0.31522	22.78	0.27	0.072
C15–C16	π	1.58683	C30–C31	π*	0.35998	20.51	0.27	0.067
C17–N19	π	1.70448	C20–N24	π*	0.59018	36.88	0.27	0.097
C20–N24	π	1.77433	N6–C23	π*	0.44773	31.58	0.31	0.094
C21–C22	π	1.59826	C20–N24	π*	0.59018	33.53	0.21	0.079
			C33–C36	π*	0.28438	21.33	0.28	0.071
			C34–C35	π*	0.36126	20.11	0.26	0.066
C25–C26	π	1.69356	C9–C10	π*	0.45947	18.82	0.29	0.069
N13	σ	1.89272	C11–N12	σ*	0.04851	16.41	0.72	0.099
C25–C26	π	1.69356	C27–C28	π*	0.36162	21.84	0.27	0.070
C37–H48	σ	1.97561	C2–C3	σ*	0.02721	5.89	1.05	0.070
N6	σ	1.89283	C1–N5	σ*	0.04891	16.34	0.72	0.098
C56–O74	σ	1.98418	C54–C55	σ*	0.02277	2.63	1.40	0.054
Zn41		0.29469	C23–N24	σ*	0.04884	6.73	0.10	0.057
C77–H80	σ	1.97498	C76–C78	σ*	0.02543	5.99	1.05	0.071
			C79–C83	σ*	0.01638	4.83	1.05	0.064
C115–C117	π	1.66355	C110–C112	π*	0.35522	21.78	0.28	0.070
C128–O144	σ	1.97915	C145–C147	σ*	0.02472	2.76	1.33	0.054
			C30–O144	σ*	0.03672	3.79	0.92	0.053
C30	σ	1.99883	C128–O144	σ*	0.07685	1.75	10.35	0.122
C90	σ	1.99864	C94–O108	σ*	0.03577	1.42	10.42	0.109
N5	σ	1.82582	N12	σ*	0.00312	5.20	2.06	0.097
			N18	σ*	0.00316	7.42	2.05	0.115
O108	π	1.82676	C89–C90	π*	0.40919	19.47	0.36	0.079
O109	π	1.85958	C27–C28	π*	0.36162	25.19	0.33	0.087
O143	π	1.81169	C124–C125	π*	0.40932	23.82	0.35	0.086
			C129–C130	π*	0.40967	23.72	0.35	0.086

Table 6 (continued)

NBO(i)	Type	ED/e	NBO(j)	Type	ED//e	$E(2)^a$(Kcal/mol)	$E(j)–E(i)^b$(a.u.)	$F(i,j)^c$(a.u)
N5	σ	1.82582	Zn41		0.00096	15.69	5.89	0.284
N12	σ	1.82577	Zn41		0.29469	48.86	0.70	0.170
Zn41		0.29469	N5	σ*	0.00312	23.59	1.36	0.414
			N12	σ*	0.00312	23.58	1.36	0.414
			N18	σ*	0.00316	23.42	1.35	0.411
			N24	σ*	0.00053	23.60	1.36	0.414
			C1–N5	σ*	0.04891	6.93	0.10	0.057
			C17–N18	σ*	0.04882	6.77	0.10	0.057

Natural bond orbital (NBO) and non-linear optics (NLO) analysis

The NBO analysis was used to calculate the $E^{(2)}$ stabilization energies showing the displacement of the electron between the donor–acceptor and the atomic charge distribution of the phthalocyanine compound. The natural bond orbital (NBO) analysis technique provides a suitable basis for investigating the interaction of bonds in the molecule and charge transfers (Hakiri et al. 2018; Halim and Khalil 2017; Ravaei et al. 2019). The parameters for compound (**4**) $\mu = 0.9611$ D, $\alpha = -681.84$ au, and $\beta = 3.6 \times 10^{-21}$ esu were found in gas phase. These values for the M-Pc molecules examined indicate that they can be considered as NLO materials (Table 6).

The NBO calculation used the theoretical calculation to understand a second interaction between the filled orbitals of a subsystem and the empty orbitals of another subsystem. These results are delocalization and hyperconjugation measurements.

The total stabilization energies of N6–C23 (occ. 1.70249)—C1–N5 (occ. 0.59327) $\pi \rightarrow \pi^*$ are 36.85 kcal mol^{-1}, C1–N6 (occ. 1.98029)—C22–C23 (occ. 0.04202) $\sigma \rightarrow \sigma^*$ 3.37 kcal mol^{-1} and C8–N12 (occ. 1.77064) C9–C10 (occ. 0.45947) $\pi \rightarrow \pi^*$ 52.99 kcal mol − 1. As an example of the electronic transitions in the phthalocyanine nucleus, the stabilization energy was found as LP Zn41 (occ. 0.29469) N5, N12, N18, N24 $\rightarrow \sigma^*$ 23.42–23.60 kcal mol^{-1}. The high values of $E^{(2)}$ stabilization energies from the NBO analysis of the metallo phthalocyanine compounds indicate the stability and π-electrons delocalization of the molecules. Interactions between orbitals in the molecule or stabilization energy are important in predicting molecular charge-transfer interactions. The natural electron configuration of Zn-Pc was calculated as $Zn41 = [core]\ 4\ s^{(0.39)}\ 3d^{(9.93)}\ 4p^{(0.01)}$.

Conclusions

The (9-phenyl-9H-xanthen-9-yl) oxy substituted zinc phthalocyanine and its starting material were synthesized for the first time in this study by a low-cost method. The synthesized compounds are described by the conventional spectroscopic methods such as IR, UV–Vis, and NMR. The fluorescence of the synthesized phthalocyanine compound and its non-aggregation property makes it advantageous for applications. Fluorescence Stokes shift value of zinc phthalocyanine was found to be consistent with the literature value. The DFT/B3LYP calculation method was used to analyze the 6-311G and LanL2DZ base clusters. After optimizing the structure and obtaining the bond lengths and angles between the core metal atom and the polarizability, the dipole moment was determined. The electron transfer between the orbital levels and the energy gap between these levels were investigated. It was also observed that the experimental results coincide with the calculated results. Experimentally and computationally described new zinc phthalocyanine compound can be regarded a useful candidate for many technological products using phthalocyanines.

Acknowledgements This study was supported by the Scientific Research Projects Unit of Van Yuzuncu Yıl University (FDK-2019-8105).

References

Abkari A, Chaabane I, Guidara K (2016) DFT (B3LYP/LanL2DZ and B3LYP/6311G + (d, p)) comparative vibrational spectroscopic analysis of organic–inorganic compound bis(4-acetylanilinium) tetrachlorocuprate(II). Physica E Low Dimens Syst Nanostruct 81:136–144. https://doi.org/10.1016/j.physe.2016.03.010

Agırtas MS (2007) Synthesis and characterization of novel symmetrical phthalocyanines substituted with four benzo [d] [1, 3] dioxol-5-ylmethoxy groups. Inorg Chim Acta 360:2499–2502. https://doi.org/10.1016/j.ica.2006.12.029

Ağırtaş MS, Yıldıko U (2008) Synthesis of new phthalocyanines substituted with four benzo[d]thiazol-2-ylthio groups. J Coord Chem 61:2781–2786. https://doi.org/10.1080/00958970801975083

Ağırtas MS, Cabir B, Özdemir S (2013) Novel metal (II) phthalocyanines with 3,4,5-trimethoxybenzyloxy-substituents: synthesis, characterization, aggregation behaviour and antioxidant activity. Dyes Pigments 96:152–157. https://doi.org/10.1016/j.dyepig.2012.07.023

Arslantaş A, Ağirtaş MS (2018) The interaction between a zinc (II) phthalocyanine compound bearing octakis phenoxyacetamide substituents and calf thymus DNA. Turk. J. Chem. 42:1310–1320. https://doi.org/10.3906/kim-1805-18

Basiuk EV, Huerta L, Basiuk VA (2019) Noncovalent bonding of 3d metal (II) phthalocyanines with single-walled carbon nanotubes: a combined DFT and XPS study. Appl Surf Sci 470:622–630. https://doi.org/10.1016/j.apsusc.2018.11.159

Chen D, Wang H (2019) HOMO-LUMO energy splitting in polycyclic aromatic hydrocarbons and their derivatives. Proceedings of the Combustion Institute. 37(1):953–959. https://doi.org/10.1016/j.proci.2018.06.120

Diab N, Morales DM, Andronescu C, Masoud M, Schuhmann W (2019) A sensitive and selective graphene/cobalt tetrasulfonated phthalocyanine sensor for detection of dopamine. Sens Actuators B 285:17–23. https://doi.org/10.1016/j.snb.2019.01.022

Farahmand S, Ghiaci M, Razavizadeh JS (2019) Copper phthalocyanine as an efficient and reusable heterogeneous catalyst for direct hydroxylation of benzene to phenol under mild conditions. Inorg. Chim Acta 484:174–179. https://doi.org/10.1016/j.ica.2018.08.051

Frisch MJ, Trucks GW, Schlegel HB, Scuseria GE, Robb MA, Cheeseman JR, Scalmani G, Barone V, Mennucci B, Petersson GA, Nakatsuji H, Caricato M, Li X, Hratchian HP, Izmaylov AF, Bloino J, Zheng G, Sonnenberg JL, Hada M, Ehara M, Toyota K, Fukuda R, Hasegawa J, Ishida M, Nakajima T, Honda Y, Kitao O, Nakai H, Vreven T, Montgomery JA Jr, Peralta JE, Ogliaro F, Bearpark M, Heyd JJ, Brothers E, Kudin KN, Staroverov VN, Kobayashi R, Normand J, Raghavachari K, Rendell A, Burant JC, Iyengar SS, Tomasi J, Cossi M, Rega N, Millam MJ, Klene M, Knox JE, Cross JB, Bakken V, Adamo C, Jaramillo J, Gomperts R, Stratmann RE, Yazyev O, Austin AJ, Cammi R, Pomelli C, Ochterski JW, Martin RL, Morokuma K, Zakrzewski VG, Voth GA, Salvador P, Dannenberg JJ, Dapprich S, Daniels AD, Farkas Ö, Foresman JB, Ortiz JV, Cioslowski J, Fox DJ (2009) Gaussian 09, Revision D.01. Gaussian, Inc., Wallingford CT

Gerasymchuk Y, Guzik M, Lisiecki R, Sobczyk M, Jański J, Koll A, Boulon G, Legendziewicz J (2018) Photophysical properties and ab initio HF and DFT calculations of the structure and spectroscopy of axially chloro substituted Yb(III) monophthalocyanines in different systems. J. Luminescence 193:84–89. https://doi.org/10.1016/j.jlumin.2017.09.002

Güngördü Solğun D, Horoz S, Agırtas MS (2019) Synthesis of novel tetra (4-tritylphenoxy) substituted metallophthalocyanines and investigation of their aggregation, photovoltaic, solar cell properties. Inorg. Nano-Metal Chem. 48(10):508–514. https://doi.org/10.1080/24701556.2019.1572624

Hakiri R, Ameur I, Abid S, Derbel N (2018) Synthesis, X-ray structural, Hirshfeld surface analysis, FTIR, MEP and NBO analysis using DFT study of a 4-chlorobenzylammonium nitrate (C7ClH9N) + (NO3). J. Mol. Structure 1164:486–492. https://doi.org/10.1016/j.molstruc.2018.03.068

Halim SA, Khalil AK (2017) TD-DFT calculations, NBO analysis and electronic absorption spectra of some thiazolo[3,2-a]pyridine derivatives. J. Mol. Structure. 1147:651–667. https://doi.org/10.1016/j.molstruc.2017.06.098

Hodgkinson N, Kruger CA, Mokwena M, Abrahamse H (2017) Cervical cancer cells (HeLa) response to photodynamic therapy using a zinc phthalocyanine photosensitizer. J. Photochem Photobiol B 177:32–38. https://doi.org/10.1016/j.jphotobiol.2017

Kluson P, Drobek M, Kalaji A, Zarubova S, Krysa J, Rakusan J (2008) Singlet oxygen photogeneration efficiencies of a series of phthalocyanines in well-defined spectral regions. J. Photochemistry Photobiology A 199:267–273. https://doi.org/10.1016/j.jphotochem.2008.06.003

Krishnan MM, Baskaran S, Arumugham MN (2017) Photochemical and DFT/TD-DFT study of trifluoroethoxy substituted asymmetric metal-free and copper (II) phthalocyanines. J. Fluorine Chem. 202:1–8. https://doi.org/10.1016/j.jfluchem.2017.08.011

Laajimi M, Chaabene M, Kahouech MS, Chaabane RB, Jamoussi B, Gallot-Lavallee O (2019) Experimental and theoretical investigation on the effect of a spacer addition in zinc phthalocyanine-based anthracene properties. Physica B: Condensed Matter 565:48–60. https://doi.org/10.1016/j.physsb.2019.04.023

Li X, Zheng B-D, Peng X-H, Li S-Z, Ying J-W, Zhao Y, Huang J-D, Yoon J (2019) Phthalocyanines as medicinal photosensitizers: Developments in the last five years. Coord. Chem. Reviews. 379:147–160. https://doi.org/10.1016/j.ccr.2017.08.003

Lin H, Chen J, Zhang Y, Ulla A, Liu J, Lin F, Jiang L, Huang M (2018) Enhanced anti-microbial effect through cationization of a mono-triazatricyclodecane substituted asymmetric phthalocyanine. J. Inorg. Biochem. 189:192–198. https://doi.org/10.1016/j.jinorgbio.2018

Lv F, He X, Wu L, Liu T (2013) Lactose substituted zinc phthalocyanine: A near infrared fluorescence imaging probe for liver cancer targeting. Bioorg. Medicinal Chem. Lett. 23:1878–1882. https://doi.org/10.1016/j.bmcl.2012.12.103

Makhseed S, Bumajdad A, Ghanem B, Msayib K, McKeown NB (2004) Macrodiscotic liquid crystals derived from planar phthalocyanine oligomers. Tetrahedron Lett. 45:4865–4868. https://doi.org/10.1016/j.tetlet.2004.04.151

Nečedová MM, Martinická A, Magdolen P, Novakova V, Zahradník P (2017) Phthalocyanine-triphenylamine dyads: Synthesis, electrochemical, spectral and DFT study. Dyes Pigments 141:448–456. https://doi.org/10.1016/j.dyepig.2017.02.025

Nesterov DS, Nesterova OV, Kopylovich MN, Pombeiro AJL (2018) Pronounced retention of stereoconfiguration upon sp3 C-H bonds hydroxylation of dimethylcyclohexanes and decahydronaphthalenes with m-CPBA oxidant and a Co-phthalocyanine catalyst. Molecular Catalysis 459:8–15. https://doi.org/10.1016/j.mcat.2018.08.009

Prabhaharan M, Prabakaran AR, Gunasekaran S, Srinivasan S (2015) DFT studies on vibrational spectra, HOMO–LUMO, NBO and thermodynamic function analysis of cyanuric flüoride. Spectrochim. Acta A 136:494–503. https://doi.org/10.1016/j.saa.2014.09.062

Ravaei I, Haghighat M, Azami SM (2019) A DFT, AIM and NBO study of isoniazid drug delivery by MgO nanocage. Applied Surface Science. 469:103–112. https://doi.org/10.1016/j.apsusc.2018.11.005

Saka ET, Durmus M, Kantekin H (2011) Solvent and central metal effects on the photophysical and photochemical properties of 4-benzyloxybenzoxy substituted phthalocyanines. J. Organomet. Chem. 696:913–924. https://doi.org/10.1016/j.jorganchem.2010.10.024

Savelyev MS, Gerasimenko IY, Podgaetskii VM, Tereshchenko SA, Selishchev SV, Tolbin AY (2019) Conjugates of thermally stable phthalocyanine J-type dimers with single-walled carbon nanotubes for enhanced optical limiting applications. Opt. Laser Technol 117:272–279. https://doi.org/10.1016/j.optlastec.2019.04.036

Sayin K, Karakaş D (2015) Structural, spectral, NLO and MEP analysis of the $[MgO_2Ti_2(OPri)_6]$, $[MgO_2Ti_2(OPri)_2(acac)_4]$ and $[MgO_2Ti_2(OPri)_2(bzac)_4]$ by DFT method. Spectrochim. Acta A 144:176–182. https://doi.org/10.1016/j.saa.2015.02.086

Thimiopoulos A, Vogiatzi A, Simandiras ED, Mousdis GA, Psaroudakis N (2019) Synthesis, characterization and DFT analysis of new phthalocyanine complexes containing sulfur rich substituents. Inorg. Chim. Acta. 488:170–181. https://doi.org/10.1016/j.ica.2019.01.010

Weijer R, Broekgaarden M, Kos M, Vught R, Rauws EAJ, Breukink E, Gulik TM, Stormd G, Heger M (2015) Enhancing photodynamic therapy of refractory solid cancers: Combining second-generation photosensitizers with multi-targeted liposomal delivery. J. Photochemistry Photobiology C 23:103–131. https://doi.org/10.1016/j.jphotochemrev.2015.05.002

Wong RCH, Lo P-C, Ng DKP (2019) Stimuli responsive phthalocyanine-based fluorescent probes and photosensitizers. Coord. Chem. Reviews 379:30–46. https://doi.org/10.1016/j.ccr.2017

Yankova R, Genieva S, Dimitrova G (2017) Molecular structure, vibrational, HOMO-LUMO, MEP and NBO analysis of hafnium selenite. J. Mol. Structure. 1141:668–677. https://doi.org/10.1016/j.molstruc.2017.04.004

Zhao H, Yang Y, Shu X, Wang Y, Wu S, Ran Q, Liu J (2018) The binding of calcium ion with different groups of superplasticizers studied by three DFT methods, B3LYP, M06-2X and M06. Computational Materials Science. 152:43–50. https://doi.org/10.1016/j.commatsci.2018.05.034

Publisher's Note Springer Nature remains neutral with regard to jurisdictional claims in published maps and institutional affiliations.